Multi-static Synthetic Aperture Radar Image Formation

V. P. Krishnan
Department of Electrical, Systems and Computer Engineering
Rensselaer Polytechnic Institute
110 8th Street, Troy, NY 12180
Email: krishv2@rpi.edu

J. Swoboda
MITRE Corporation,
Bedford, MA 01730-1420
Email: jswoboda@mitre.org

C. E. Yarman
Houston Technology Center,
WesternGeco-Schlumberger,
Houston, TX 77042
Email: yarman@ecse.rpi.edu

B. Yazıcı
Department of Electrical, Systems and Computer Engineering
Rensselaer Polytechnic Institute
110 8th Street, Troy, NY 12180
Email: yazici@ecse.rpi.edu

***Abstract*—In this paper, we consider a multi-static synthetic aperture radar (SAR) imaging scenario where a swarm of airborne antennas, some of which are transmitting, receiving or both, are traversing arbitrary flight trajectories and transmitting arbitrary waveforms without any form of multiplexing. The received signal at each receiving antenna may be interfered by the scattered signals from multiple transmitters and the additive thermal noise at the receiver. Standard bi-static SAR image reconstruction algorithms result in artifacts in reconstructed images due to these interferences. In this paper, we employ microlocal analysis in a statistical setting to develop a novel filtered-backprojection (FBP) type analytic image formation method that suppresses artifacts due to interference from multiple transmitters while preserving the location and orientation of edges of the scene in the reconstructed image.**

I. Introduction

In synthetic aperture radar (SAR) imaging, a scene of interest is illuminated by electromagnetic waves that are transmitted from an antenna mounted on an airborne platform. The aim is to reconstruct an image of the scene from the measurement of the scattered waves.

In mono-static SAR, transmitter and receiver antennas are co-located. In bi-static SAR, the transmitter and receiver antennas are located on sufficiently far-apart platforms [1]. In multi-static SAR, which is the focus of this paper, multiple transmitter and receiver antennas are used to image a scene of interest. Multi-static SAR offers a variety of potential gains in scene information. The availability of multiple illumination and scattered measurements from different perspectives has the potential for improved overall resolution when the scattered measurements are fused [2]. Also some of the electronic countermeasures that have been devised for mono-static radar are less effective against distributed radar systems [3], [4]. Finally, multi-static measurements can provide better ability to distinguish targets from clutter [5].

Both bi-static and multi-static radar systems have received increased attention in recent years. A multi-static ambiguity function was recently proposed in [6]. A framework for the analysis of multi-static radar systems with multiple transmitters was introduced in [7]. An auto-focus algorithm for multi-static SAR systems using multiple transmitters is presented in [8]. In [9] a multi-static SAR image formation based on time-frequency filtering and image combination was presented. In many multi-static radar systems, it is assumed that each receiver can decompose the received signal into components due to illumination of each transmitter. This can be achieved by separating the transmitted signals by some form of multiplexing in time, frequency or coding which requires central coordination of the transmit signal parameters. In this case, the multi-static synthetic aperture image formation problem reduces to the bi-static synthetic aperture image formation problem which has been well-studied [10]-[11]. For bi-static image reconstruction algorithms involving antennas that can form narrow beam, traversing linear or circular trajectories, see [10]- [12]. For bi-static SAR image reconstruction algorithms involving antennas with poor directivity and traversing arbitrary flight trajectories, see [11], [13].

In this paper, we consider a multi-static SAR system with several transmitters and receivers traversing arbitrary, but known trajectories. We assume that the receivers *cannot* decompose the received signal according to which transmitter emitted the signal. A simple multi-static SAR scenario with two transmitters and a receiver is illustrated in Figure 1. Such a scenario emerges when the illumination is provided by sources of opportunity, such as communication satellites or cell-phone towers or when the central coordination of a swarm of antennas deployed on uninhabited aerial vehicles (UAVs) is either not possible or desirable. Bi-static reconstruction algorithms, given for example in [10] and [11], are not suited for this scenario, since they are designed for a given transmitter-receiver measurement pair and therefore result in artifacts in the reconstructed image due to interference caused by multiple transmitters.

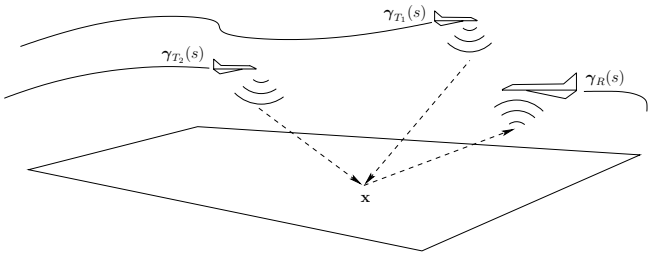

Fig. 1. Multi-static SAR geometry with two transmitters and a single receiver

In this paper, we introduce a filtered-backprojection type reconstruction algorithm for multi-static SAR with multiple transmitters transmitting arbitrary waveforms. We use microlocal analysis [14], to develop an approximate analytic image reconstruction method. Our method involves backprojecting the received data with respect to each transmitter while suppressing the interference caused by other transmitters via a suitably designed filter. We assume that we have *a priori* knowledge of the second-order statistics of the scene to be reconstructed. We determine the second-order statistics of the artifacts caused by interference based on antenna trajectories and design a filter that preserves the edges in the received data due to the scene while suppressing the artifacts induced by the interfering transmitters in the mean-square sense. We form the final image by superposition of images reconstructed for all transmitter-receiver pairs.

This paper is organized as follows: In Section II, we introduce the multi-static SAR forward model and in Section III, we focus

978-1-4244-5180-7/09/$26.00 ©2009 IEEE

on image formation and derive the filter. The numerical simulations are presented in Section IV and Section V concludes the paper. The stationary phase method based on which the filters are derived is stated in Appendix A.

II. Forward model for multi-static SAR data

We consider a multi-static SAR set-up where there are M transmitters and N receivers with $M \geq 2$ and $N \geq 1$. We index the transmitters by T_p for $p = 1, \cdots, M$ and receivers by R_q for $q = 1, \cdots, N$. Let $\boldsymbol{\gamma}_{T_p}(s)$ and $\boldsymbol{\gamma}_{R_q}(s)$ for $s \in [s_0, s_1]$ be the trajectories of the transmitters and the receivers respectively. Let $\psi : \mathbb{R}^2 \to \mathbb{R}$ be a known smooth function representing the ground topography. That is, the ground topography is given by $\mathbf{x} = (\boldsymbol{x}, \psi(\boldsymbol{x}))$ for $\boldsymbol{x} \in \mathbb{R}^2$. We assume that the electromagnetic waves propagate in free-space and then scatter in a thin region near the earth's surface. Consequently, we assume that the target reflectivity function T, is a function of the variable $\boldsymbol{x} \in \mathbb{R}^2$ [15]. Under the start-stop approximation and the single scattering Born approximation, the ideal received signal d_q at the q^{th} receiver is given by

$$d_q(s,t) = \mathcal{F}_q[T](s,t) = \sum_{p=1}^{M} \mathcal{F}_{pq}[T](s,t) \tag{1}$$

$$= \sum_{p=1}^{M} \int e^{-\mathrm{i}\omega(t - \frac{1}{c_0} R_{pq}(s,\boldsymbol{x}))} A_{pq}(\boldsymbol{x}, s, \omega) T(\boldsymbol{x}) \mathrm{d}\boldsymbol{x} \mathrm{d}\omega,$$

where $s \in [s_0, s_1]$ is the *slow-time* variable, $t \in [t_0, t_1]$ is the *fast-time* variable,

$$R_{pq}(s, \boldsymbol{x}) = |\mathbf{x} - \boldsymbol{\gamma}_{T_p}(s)| + |\mathbf{x} - \boldsymbol{\gamma}_{R_q}(s)|, \tag{2}$$

is the total distance from the transmitter position $\boldsymbol{\gamma}_{T_p}(s)$ to $\mathbf{x}$ and from $\mathbf{x}$ to the receiver position $\boldsymbol{\gamma}_{R_q}(s)$, c_0 is the speed of light in free-space, ω is the temporal frequency and $A_{pq}(\boldsymbol{x}, s, \omega)$ is a function that takes into account the transmitter and receiver antenna beam patterns, the transmitted waveforms and geometrical spreading factors [16]. We assume that the functions $A_{pq}(\boldsymbol{x}, s, \omega)$ for $p = 1, \cdots, M$ and $q = 1, \cdots, N$ satisfy the following estimate for some real number m_{pq}:

$$|\partial_\omega^\alpha \partial_s^\beta \partial_{x_1}^{\rho_1} \partial_{x_2}^{\rho_2} A_{pq}(\boldsymbol{x}, s, \omega)| \leq C(1 + |\omega|^2)^{(m_{pq} - |\alpha|)/2}, \tag{3}$$

for $(\boldsymbol{x}, s) \in K$ and $\omega \in \mathbb{R}$. Here $K \subset \mathbb{R}^2 \times \mathbb{R}$ is any compact set and α and β, ρ_1, ρ_2 are any non-negative integers, and C is a constant in terms of $p, q, K, \alpha, \beta, \rho_1, \rho_2$. These estimates are satisfied when the antenna is broadband and when the source waveform is a band limited waveform. These assumptions are needed to make various stationary phase calculations. Furthermore, these assumptions make each operator $\mathcal{F}_{pq}$ a *Fourier Integral Operator* [17].

The multi-static SAR image formation problem involves reconstruction of the target reflectivity function T using the data $d_q(s,t)$ for $s \in [s_0, s_1]$, $t \in [t_0, t_1]$ and $q = 1, \cdots, N$ based on the model (1).

In the presence of noise, we consider the following model for the measurement at the q^{th} receiver:

$$d_q(s,t) = \mathcal{F}_q[T](s,t) + n_q(s,t). \tag{4}$$

We assume both the scene T and noise n_q, $q = 1, \ldots, N$ are statistically uncorrelated stochastic processes, whose means, without loss of generality, are zero. Here $\mathcal{F}_q$ is defined as in (1).

Furthermore, we assume that T is stationary, and n_q is statistically uncorrelated in slow-time variable s and stationary in fast-time variable t. Thus

$$\widetilde{S}_T(\zeta, \zeta') = S_T(\zeta)\delta(\zeta - \zeta') \tag{5}$$

and

$$\widetilde{S}_{n_q}(s, \omega, s', \omega') = S_{n_q}(\omega, s)\delta(s - s')\delta(\omega - \omega'), \tag{6}$$

where

$$\widetilde{S}_T(\zeta, \zeta') = \frac{1}{(2\pi)^4} \int e^{\mathrm{i}(\boldsymbol{x}\cdot\zeta - \boldsymbol{x}'\cdot\zeta')} R_T(\boldsymbol{x}, \boldsymbol{x}') \mathrm{d}\boldsymbol{x} \mathrm{d}\boldsymbol{x}' \tag{7}$$

and

$$\widetilde{S}_{n_q}(s, \omega, s', \omega') = \frac{1}{(2\pi)^2} \int e^{\mathrm{i}(\omega t - \omega' t')} R_{n_q}(s, t, s', t') \mathrm{d}t \mathrm{d}t', \tag{8}$$

where R_T and R_{n_q} are the auto-covariance functions of T and n_q, respectively. S_T and S_{n_q} are referred to as the power spectral density functions of T and n_q respectively.

III. Image Formation

We define the set of filtered-backprojection operators, $\mathcal{K}_{pq}$, for the multi-static data at the q^{th} receiver with respect to each transmitter p, $p = 1, \cdots, M$ as follows:

$$\widehat{T}_{pq}(\boldsymbol{z}) := \mathcal{K}_{pq} d_q(\boldsymbol{z}) := \int e^{\mathrm{i}\omega(t - \frac{1}{c_0} R_{pq}(s,z))} \times \tag{9}$$

$$\times B_{pq}(\boldsymbol{z}, s, \omega) D_q(s, \omega) \mathrm{d}s \mathrm{d}\omega, \tag{10}$$

where

$$D_q(s, \omega) = \sum_{p=1}^{M} \int e^{\mathrm{i}\frac{\omega}{c_0} R_{pq}(s,\boldsymbol{x})} A_{pq}(\boldsymbol{x}, s, \omega) T(\boldsymbol{x}) \mathrm{d}\boldsymbol{x}. \tag{11}$$

Here B_{pq} for $q = 1, \cdots, N$ and $p = 1, \cdots, M$ are the filters to be determined below.

Substituting the multi-static data model given in (1), we obtain

$$\widehat{T}_{pq}(\boldsymbol{z}) = \widehat{T}^p_{pq}(\boldsymbol{z}) + \sum_{r=1, r\neq p}^{M} \widehat{T}^r_{pq}(\boldsymbol{z}) + \mathcal{K}_{pq}[n_q](\boldsymbol{z}) \tag{12}$$

where $\widehat{T}^p_{pq}(\boldsymbol{z}) = \mathcal{K}_{pq}\mathcal{F}_{pq}[T](\boldsymbol{z})$ and $\widehat{T}^r_{pq}(\boldsymbol{z}) = \mathcal{K}_{pq}\mathcal{F}_{rq}[T](\boldsymbol{z})$, for $r = 1, \cdots, M, r \neq p$. Note that $\mathcal{K}_{pq}\mathcal{F}_{pq}$ is exactly the imaging operator that appears in the bi-static image reconstruction [11]. This is a pseudodifferential operator and since pseudodifferential operators have pseudolocal property, they put the edges of the target T at the right location and right orientation in $\widehat{T}_{pq}(\boldsymbol{z})$. Now $\mathcal{K}_{pq}\mathcal{F}_{rq}[T]$ for $p \neq r = 1, \cdots, M$ involves backprojection of the ideal received signal at the q^{th} receiver due to the r^{th} transmitter for $r \neq p$. The operators $\mathcal{K}_{pq}\mathcal{F}_{rq}$ for $r \neq p$ are in general not pseudodifferential operators and hence the edges of T are not reconstructed at the right location and orientation.

We design the filters B_{pq} to minimize the mean-square error

$$I(B_{pq}) = \mathrm{E}\left[\int |\widehat{T}_{pq}(\boldsymbol{z}) - T_{\Omega^{pq}_{\boldsymbol{z}}}(\boldsymbol{z})|^2 \mathrm{d}\boldsymbol{z}\right], \tag{13}$$

where E is the expectation operator,

$$T_{\Omega^{pq}_{\boldsymbol{z}}}(\boldsymbol{z}) = \mathcal{I}_{\Omega^{pq}_{\boldsymbol{z}}} T(\boldsymbol{z}) = \int_{\Omega^{pq}_{\boldsymbol{z}}} \mathrm{e}^{\mathrm{i}(\boldsymbol{x} - \boldsymbol{z})\cdot\boldsymbol{\xi}} T(\boldsymbol{x}) \mathrm{d}\boldsymbol{x} \mathrm{d}\boldsymbol{\xi} \tag{14}$$

is the best possible image that could be reconstructed by the transmitter-receiver pair (p, q) [11]. Here

$$\Omega^{pq}_{\boldsymbol{z}} = \{\boldsymbol{\xi} = \frac{\omega}{c_0} \Sigma_{pq}(s, \boldsymbol{z}, \boldsymbol{z}) : A_{pq}(\boldsymbol{z}, s, \omega) \neq 0\} \tag{15}$$

with

$$\Sigma_{pq}(s,\boldsymbol{z},\boldsymbol{z}) = [D(\boldsymbol{z}_1,\boldsymbol{z}_2)]^T \left((\widehat{\boldsymbol{\gamma}_{T_p}(s)-\boldsymbol{z}}) + (\widehat{\boldsymbol{\gamma}_{R_q}(s)-\boldsymbol{z}}) \right), \tag{16}$$

with

$$D(\boldsymbol{z}_1,\boldsymbol{z}_2) = \begin{pmatrix} 1 & 0 \\ 0 & 1 \\ \frac{\partial\psi}{\partial \boldsymbol{z}_1} & \frac{\partial\psi}{\partial \boldsymbol{z}_2} \end{pmatrix}. \tag{17}$$

Here $(\widehat{\boldsymbol{\gamma}_{T_p}(s)-\boldsymbol{z}})$ and $(\widehat{\boldsymbol{\gamma}_{R_q}(s)-\boldsymbol{z}})$ denote unit vectors in the direction of $\boldsymbol{\gamma}_{T_p}(s)-\boldsymbol{z}$ and $\boldsymbol{\gamma}_{R_q}(s)-\boldsymbol{z}$ respectively.

In other words $\Sigma_{pq}(s,\boldsymbol{z},\boldsymbol{z})$ is the projection of the bisector of $(\widehat{\boldsymbol{\gamma}_{T_p}(s)-\boldsymbol{z}})$ and $(\widehat{\boldsymbol{\gamma}_{R_q}(s)-\boldsymbol{z}})$ onto the tangent plane of the ground topography at $\boldsymbol{z}$.

Expanding the right hand side of (13), under the assumption that n_q and T are statistically uncorrelated, we obtain

$$\begin{aligned} I(B_{pq}) = & \underbrace{\mathrm{E}[\int |\widehat{T}^p_{pq}(\boldsymbol{z}) - T_{\Omega^{pq}_z}(\boldsymbol{z})|^2 \mathrm{d}\boldsymbol{z}]}_{I_1} \\ & + \underbrace{\mathrm{E}[\int |\sum_{r=1,r\neq p}^{M} \widehat{T}^r_{pq}(\boldsymbol{z})|^2 \mathrm{d}\boldsymbol{z}]}_{I_2} + \underbrace{\mathrm{E}[\int |\mathcal{K} n_q(\boldsymbol{z})|^2 \mathrm{d}\boldsymbol{z}]}_{I_3} \\ & + \underbrace{2\mathrm{E}[\sum_{r=1,r\neq p}^{M} \mathrm{Re} \int (\widehat{T}^p_{pq}(\boldsymbol{z}) - T_{\Omega^{pq}_z}(\boldsymbol{z}))\overline{\widehat{T}^r_{pq}} \mathrm{d}\boldsymbol{z}]}_{I_4}. \end{aligned} \tag{18}$$

For simplicity, we write $I = I_1 + I_2 + I_3 + I_4$.

Using the change of variables

$$(s,\omega) \to \boldsymbol{\xi} = \frac{\omega}{c_0}\Sigma_{pq}(s,\boldsymbol{z},\boldsymbol{z}), \tag{19}$$

and linearizing the phase around $\boldsymbol{x} = \boldsymbol{z}$, we obtain

$$\widehat{T}^p_{pq}(\boldsymbol{z}) = \int \mathrm{e}^{\mathrm{i}(\boldsymbol{x}-\boldsymbol{z})\cdot\boldsymbol{\xi}} B_{pq}(\boldsymbol{z},\boldsymbol{\xi}) A_{pq}(\boldsymbol{z},\boldsymbol{\xi}) |J_{pq}(\boldsymbol{x},\boldsymbol{z},\boldsymbol{\xi})| T(\boldsymbol{x}) \mathrm{d}\boldsymbol{x}\mathrm{d}\boldsymbol{\xi}, \tag{20}$$

where J_{pq} is the Jacobian of the inverse of the transformation (19) and

$$\begin{aligned} \widehat{T}^r_{pq}(\boldsymbol{z}) = & \int e^{\mathrm{i}(\boldsymbol{x}-\boldsymbol{z})\cdot\boldsymbol{\xi}} B_{pq}(\boldsymbol{z},\boldsymbol{\xi}) A_{rq}(\boldsymbol{x},\boldsymbol{\xi}) |J_{pq}(\boldsymbol{x},\boldsymbol{z},\boldsymbol{\xi})| \times \\ & \times \tilde{T}_r(\boldsymbol{x},\xi) \mathrm{d}\boldsymbol{x}\mathrm{d}\boldsymbol{\xi}, \end{aligned} \tag{21}$$

where

$$\widetilde{T}_r(\boldsymbol{x},\boldsymbol{\xi}) := \widetilde{T}_r(\boldsymbol{x}, s(\boldsymbol{\xi}), \omega(\boldsymbol{\xi})) = e^{\mathrm{i}\triangle_{rp}(\boldsymbol{x},s(\boldsymbol{\xi}),\omega(\boldsymbol{\xi}))} T(\boldsymbol{x}) \tag{22}$$

and

$$\triangle_{rp}(\boldsymbol{x},s(\boldsymbol{\xi}),\omega(\boldsymbol{\xi})) = \frac{\omega(\boldsymbol{\xi})}{c_0}\Big(|\mathbf{x} - \boldsymbol{\gamma}_{T_r}(s(\boldsymbol{\xi}))| - |\mathbf{x} - \boldsymbol{\gamma}_{T_p}(s(\boldsymbol{\xi}))| \Big). \tag{23}$$

Using the method of stationary phase, we approximate each of the integrals I_1, I_2 as follows:

$$I_1 \approx \int |B_{pq}(\boldsymbol{x}',\boldsymbol{\zeta}) A_{pq}(\boldsymbol{x}',\boldsymbol{\zeta}) |J_{pq}(\boldsymbol{x}',\boldsymbol{x}',\boldsymbol{\zeta})| - 1|^2 S_T(\boldsymbol{\zeta}) \mathrm{d}x' \mathrm{d}\boldsymbol{\zeta}. \tag{24}$$

$$\begin{aligned} I_2 \approx & \sum_{r=1,r\neq p}^{M} \int |A_{rq}(\boldsymbol{x}',\boldsymbol{\zeta}) B_{pq}(\boldsymbol{x}',\boldsymbol{\zeta}) J_{pq}(\boldsymbol{x}',\boldsymbol{x}',\boldsymbol{\zeta})|^2 \\ & \times S_T(\boldsymbol{\zeta} + \partial_{\boldsymbol{x}'} \triangle_{rp}(0,\boldsymbol{\zeta})) \mathrm{d}\boldsymbol{x}' \mathrm{d}\boldsymbol{\zeta}. \end{aligned} \tag{25}$$

Using the change of variables (19) and condition (6), we obtain

$$I_3 \approx \int |B_{pq}(\boldsymbol{z},\boldsymbol{\zeta})|^2 S_n(\boldsymbol{\zeta}) |J(\boldsymbol{z},\boldsymbol{z},\boldsymbol{\zeta})| \mathrm{d}\boldsymbol{z}\mathrm{d}\boldsymbol{\zeta}. \tag{26}$$

The assumption of stationarity of T implies that the leading order contribution of I_4 to $I(B_{pq})$ is 0. Therefore $I_4 \approx 0$ does not contribute to the determination of the filter B_{pq}. Thus

$$I(B_{pq}) \approx I_1 + I_2 + I_3. \tag{27}$$

Substituting I_1, I_2 and I_3 given by (24), (25) and (26), respectively, into I, and then equating the variational derivative of I with respect to B_{pq} to zero, we obtain

$$B_{pq}(\boldsymbol{x},\boldsymbol{\zeta}) = \frac{\chi_{\Omega^{pq}_x}(\boldsymbol{x},\boldsymbol{\zeta}) \overline{A_{pq}(\boldsymbol{x},\boldsymbol{\zeta})} S_T(\boldsymbol{\zeta})}{|J_{pq}(\boldsymbol{x},\boldsymbol{x},\boldsymbol{\zeta})| \times \text{Dr.} + S_{n_q}(\boldsymbol{\zeta})}, \tag{28}$$

where

$$\text{Dr.} = |A_{pq}(\boldsymbol{x},\boldsymbol{\zeta})|^2 S_T(\boldsymbol{\zeta}) + \sum_{r=1,r\neq p}^{M} |A_{rq}(\boldsymbol{x},\boldsymbol{\zeta})|^2 S_T(\boldsymbol{\zeta} + \partial_{\boldsymbol{x}} \triangle_{rq}(0,\boldsymbol{\zeta})).$$

Here $\chi_{\Omega^{pq}_x}$ is a smooth cut-off function such that it is identically 1 in the interior of the data collection manifold Ω^{pq}_x and 0 outside.

IV. Numerical Simulations

In our numerical simulations, we considered a scene of size $[0,22]\times[0,22]$ km^2 with a square target of length 5.5 km with center at $(8.8, 12)$ and a rectangular target of size 3.3 km×8.8 km with center located at $(15.4, 10)$ (see Figure 2). The scene was discretized to a 128×128 grid of pixels with $(0,0)$ and $(22,22)$ corresponding to pixel numbers $(1,1)$ and $(128,128)$ respectively.

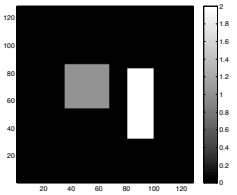

Fig. 2. Scene used in numerical simulations

We used a discrete version of the multi-static forward data model (Equation (4)) to generate our simulation data. We made the assumptions that the earth's surface is flat and the amplitude functions $A_{pq} \equiv 1$. This choice of amplitude functions corresponds to isotropic transmitters and receivers using a delta function as the transmit waveform. The parameters we used correspond to a system bandwidth of approximately 0.873 MHz.

We performed several sets of numerical simulations in our paper, [19]. Here we have included two simulations from [19] with transmitters and receivers traversing a circular flight trajectory, $\boldsymbol{\gamma}_c(s) = (11 + 22\cos s, 11 + 22\sin s, 6.5)$: (1) Three transmitters and one receiver on the circular path and (2) two transmitters and one receiver on a circular path with noise added to the received data.

We determined the spectrum of the target by numerically correlating the target image with itself and then taking the fast Fourier transform of the resultant correlation. For the simulation in which the received data is corrupted with noise, we chose the following wide-band noise model, since the transmitted pulse is an ideal wide-band signal:

$$S_n(s,\omega) = \frac{1}{1+|\omega|^5} \frac{\pi/5}{\sin(\pi/5)}. \tag{29}$$

The signal-to-noise ratio (SNR) we used is defined by

$$\mathrm{SNR} = 20 \log \frac{\frac{1}{N_d} \sum_{i=1}^{N_d} (d(s_i, t_i) - \mu_d)^2}{E[||n||^2]} \mathrm{dB}, \tag{30}$$

where N_d is the number of grid points and μ_d is the mean value of the radar data.

Recall that the multi-static reconstruction scheme of this paper fixes a transmitter-receiver pair, uses the filter defined in Equation (28) to reconstruct the image and then obtain the final image by superposition of the reconstructed images for all transmitter-receiver pairs. In our simulations, we compared this multi-static reconstruction scheme with the bi-static reconstruction method of [11].

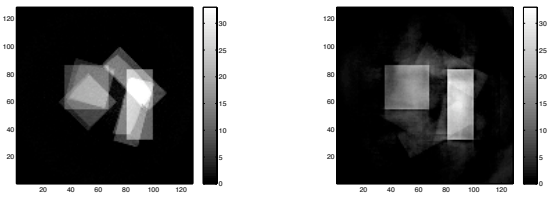

(a) (b)

Fig. 3. Multi-static set-up with three transmitters $\boldsymbol{\gamma}_{T_1}(s) = (11 + 22\cos s, 11 + 22\sin s, 6.5)$, $\boldsymbol{\gamma}_{T_2}(s) = (11 + 22\cos(s + 2\pi/3), 11 + 22\sin(s+2\pi/3), 6.5)$ and $\boldsymbol{\gamma}_{T_3}(s) = (11+22\cos(s+\pi/6), 11+22\sin(s+\pi/6), 6.5)$, and one receiver $\boldsymbol{\gamma}_R(s) = (11+22\cos(s+\pi/3), 11+22\sin(s+\pi/3), 6.5)$. (a) Reconstruction from the bi-static FBP algorithm of [11] with respect to Transmitter 3. (b) The image reconstructed by the multi-static scheme of this paper.

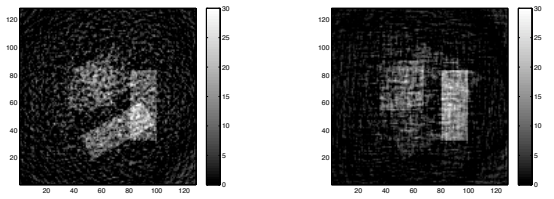

(a) (b)

Fig. 4. Multi-static set-up with two transmitters and one receiver with additive noise at an SNR of 0 dB. The flight trajectories are $\boldsymbol{\gamma}_{T_1}(s) = (11+22\cos s, 11+22\sin s, 6.5)$, $\boldsymbol{\gamma}_{T_2}(s) = (11+22\cos(s+2\pi/3), 11+22\sin(s+2\pi/3), 6.5)$, and $\boldsymbol{\gamma}_R(s) = (11+22\cos(s+\pi/3), 11+22\sin(s+\pi/3), 6.5)$ (a) Reconstruction of the target scene for data corrupted with additive noise of SNR $= 0$ dB using the bi-static FBP scheme of [18] with respect to transmitter T_2. (b) Reconstruction from the multi-static algorithm of this paper.

V. Conclusion

In this paper, we developed an FBP-type synthetic-aperture radar inversion method for multi-static SAR with multiple transmitters transmitting arbitrary waveforms. These waveforms could be overlapping in time and frequency and have no form of multiplexing. To the best of our knowledge, our work is the first in the literature that can produce multi-static SAR images while suppressing the artifacts caused by multiple interfering transmitters. We demonstrated the performance of the inversion method in numerical simulations, which is in correspondence with theoretical expectations.

While our paper has focused primarily on image formation for multi-static SAR, the techniques are also applicable to other imaging problems such as those arising in acoustics, geophysics and tomography.

Appendix A
Stationary phase method

Let u be a smooth function of compact support in $\mathbb{R}^n$ and let φ be a real valued function with only non-degenerate critical points. A point $x_0 \in \mathbb{R}^n$ is called a non-degenerate critical point if $D\varphi(x_0) = 0$ and the Hessian matrix $D^2\varphi(x_0)$ has non-zero determinant. The stationary phase theorem states that as $\lambda \to \infty$,

$$\int e^{\mathrm{i}\lambda\varphi(\boldsymbol{x})} u(\boldsymbol{x}) \mathrm{d}\boldsymbol{x} = (\frac{2\pi}{\lambda})^{\frac{n}{2}} \sum_{\{\boldsymbol{x}_0 : D\varphi(\boldsymbol{x}_0)=0\}} \frac{e^{\mathrm{i}\lambda\varphi(\boldsymbol{x}_0)} e^{\mathrm{i}\frac{\pi}{4}\mathrm{sgn}D^2\varphi(\boldsymbol{x}_0)}}{\sqrt{|\det D^2\varphi(\boldsymbol{x}_0)|}} u(x_0) + \\ + \mathcal{O}(\lambda^{-\frac{n}{2}-1}). \tag{31}$$

References

[1] N. J. Willis, *Bistatic Radar*. Norwood, MA: Artech House, 1991.

[2] S. R. Doughty, K. Woodbridge, and C. J. Baker, "Improving resolution using multistatic radar," *Radar Systems, 2007 IET International Conference on*, pp. 1–5, Oct. 2007.

[3] W. Goj, *Synthetic Aperture Radar and Electronic Warfare*. Boston: Artech House, 1993.

[4] A. M. Horne and G. Yates, "Bistatic synthetic aperture radar," in *Proceedings of IEEE Radar Conference*, Oct. 2002, pp. 6 – 10.

[5] L. M. H. Ulander and T. Martin, "Bistatic ultrawideband SAR for imaging of ground targets under foliage," in *Proceedings of 2005 IEEE Radar Conference*, May 2005, pp. 419 – 423.

[6] I. Bradaric, G. T. Capraro, and M. C. Wicks, "Waveform diversity for different multistatic radar configurations," *Signals, Systems and Computers, 2007. ACSSC 2007. Conference Record of the Forty-First Asilomar Conference on*, pp. 2038–2042, Nov. 2007.

[7] I. Bradaric, G. T. Capraro, D. D. Weiner, and M. C. Wicks, "A framework for the analysis of multistatic radar systems with multiple transmitters," *Electromagnetics in Advanced Applications, 2007. ICEAA 2007. International Conference on*, pp. 443–446, Sept. 2007.

[8] K.-H. Liu and D. C. Munson, "Autofocus in multistatic passive SAR imaging," *Acoustics, Speech and Signal Processing, 2008. ICASSP 2008. IEEE International Conference on*, pp. 1277–1280, 31 2008-April 4 2008.

[9] T. Teer and N. A. Goodman, "Multistatic SAR algorithm with image combination," *Radar, 2006 IEEE Conference on*, pp. 8 pp.–, April 2006.

[10] O. Arikan and D. C. M. Jr., "A tomographic formulation of bistatic synthetic aperture radar," in *Proceedings of ComCon ï£¡88*, Oct. 1988, p. 418.

[11] C. E. Yarman, B. Yazıcı, and M. Cheney, "Bistatic synthetic aperture radar imaging for arbitrary flight trajectories," *Image Processing, IEEE Transactions on*, vol. 17, no. 1, pp. 84–93, Jan. 2008.

[12] M. Soumekh, "Bistatic synthetic aperture radar inversion with application in dynamic object imaging," *IEEE Transactions on Signal Processing*, vol. 39, pp. 2044–2055, Sept. 1991.

[13] M. Cheney and B. Yazıcı, "Radar imaging with independently moving transmitters and receivers," in *Proceedings of Defense Advance Signal Processing (DASP) Workshop*, Dec. 2006.

[14] A. Grigis and J. Sjöstrand, *Microlocal analysis for differential operators*, ser. London Mathematical Society Lecture Note Series. Cambridge: Cambridge University Press, 1994, vol. 196, an introduction.

[15] C. J. Nolan and M. Cheney, "Synthetic aperture inversion for arbitrary flight paths and non-flat topography," *IEEE Transactions on Image Processing*, vol. 12, pp. 1035–1043, 2003.

[16] M. Cheney, "Synthetic-aperture assessment of a dispersive surface," *International Journal of Imaging Systems and Technology*, vol. 14, pp. 28–34, 2004.

[17] J. J. Duistermaat, *Fourier integral operators*, ser. Progress in Mathematics. Boston, MA: Birkhäuser Boston Inc., 1996, vol. 130.

[18] J. Swoboda, C. E. Yarman, and B. Yazıcı, "Bistatic synthetic aperture radar imaging for arbitrary trajectories in the presence of noise and clutter", To appear in SPIE Defense and Security Conference, Apr. 2009.

[19] V. P. Krishnan, J. Swoboda, C. E. Yarman, and B. Yazıcı. "Multi-static synthetic aperture radar image formation", Accepted for publication in IEEE Transactions on Image Processing.